Biophysical Journal
Article

Biophysical Society

Collective polymerase dynamics emerge from DNA supercoiling during transcription

Stuart A. Sevier[1,2] and Sahand Hormoz[1,2,3,*]
[1]Department of Systems Biology, Harvard Medical School, Boston, Massachusetts; [2]Department of Data Sciences, Dana-Farber Cancer Institute, Boston, Massachusetts; and [3]Broad Institute of MIT and Harvard, Cambridge, Massachusetts

ABSTRACT All biological processes ultimately come from physical interactions. The mechanical properties of DNA play a critical role in transcription. RNA polymerase can over or under twist DNA (referred to as DNA supercoiling) when it moves along a gene, resulting in mechanical stresses in DNA that impact its own motion and that of other polymerases. For example, when enough supercoiling accumulates, an isolated polymerase halts, and transcription stops. DNA supercoiling can also mediate nonlocal interactions between polymerases that shape gene expression fluctuations. Here, we construct a comprehensive model of transcription that captures how RNA polymerase motion changes the degree of DNA supercoiling, which in turn feeds back into the rate at which polymerases are recruited and move along the DNA. Surprisingly, our model predicts that a group of three or more polymerases move together at a constant velocity and sustain their motion (forming what we call a polymeton), whereas one or two polymerases would have halted. We further show that accounting for the impact of DNA supercoiling on both RNA polymerase recruitment and velocity recapitulates empirical observations of gene expression fluctuations. Finally, we propose a mechanical toggle switch whereby interactions between genes are mediated by DNA twisting as opposed to proteins. Understanding the mechanical regulation of gene expression provides new insights into how endogenous genes can interact and informs the design of new forms of engineered interactions.

SIGNIFICANCE All biological processes come from physical interactions. During gene expression, RNA polymerase moves along DNA and generates a messenger RNA copy of DNA. Because DNA has a helical structure, polymerase needs to twist the DNA to move along it. Over and under twisting of DNA change the mechanical properties of DNA. We present a model that captures how movement of a polymerase changes excess twist within DNA, which in turn feeds back into the rate at which polymerases move. Our model predicts that twisting of DNA generates effective interactions between polymerases such that three or more polymerases can keep moving along DNA, whereas one or two polymerases are halted. These interactions can explain observed fluctuations in gene expression.

INTRODUCTION

Numerous physical processes contribute to gene expression (1). For example, transcription, an essential step in gene expression where DNA is converted to RNA, has a mechanical component. During transcription, an RNA polymerase can twist DNA and generate stresses on DNA (2,3) that impact its own motion and that of other polymerases (4) affecting gene expression (5). Therefore, to understand the dynamics of gene expression, we need to account for the mechanical nature of transcription (6).

DNA forms a right-handed helix from two complementary strands of nucleic acid chains. The number of times these two chains wind around each other is a topological quantity called the linking number (7). DNA supercoiling is a change in the natural linking number of DNA (the number of times the two DNA strands wind around each other in a relaxed configuration). DNA supercoiling is intimately linked to transcription (8) and can control both the rate at which polymerases are recruited and the rate at which polymerases move along DNA (4,5). Gene expression occurs in a stochastic ("bursty") manner (9). Early insights into gene expression fluctuations (10–14) and RNA polymerase cooperation (15) led to numerous phenomenological models that linked bursting to intrinsic polymerase pausing (16–19), pushing (20), and barrier encounters (21). These models were followed by theoretical

Submitted April 11, 2022, and accepted for publication September 22, 2022.
*Correspondence: sahand_hormoz@hms.harvard.edu
Editor: Jason Kahn.
https://doi.org/10.1016/j.bpj.2022.09.026

(22–24) and experimental studies (25–27) that explicitly considered the role of DNA supercoiling as a mechanism of transcriptional bursting. In addition to influencing fluctuations, experimental (28) and theoretical (22,23) observations have shown that DNA supercoiling can halt isolated polymerases and stop transcription nonlocally, whereas multiple polymerases can undergo sustained motion (4,29,30) and influence the recruitment of polymerases to neighboring promoters (31). Despite the advances that these studies have made, we still lack a comprehensive framework that captures how DNA twisting by RNA polymerase during transcription feeds back into the recruitment and motion of other RNA polymerases, which in turn change the local excess twist within DNA.

Here, we construct a model of mechanical aspects of gene expression that captures the feedback cycle between DNA twisting and RNA polymerase recruitment and motion. Within our framework, multiple polymerases interact nonlocally via twisting of DNA generated by the movement of the polymerases along the gene. We show that these interactions play a key role in setting the velocity at which polymerases can move along a gene, which in turn sets the degree of gene expression fluctuations. Surprisingly, we demonstrate that three or more interacting polymerases undergo sustained motion, whereas isolated polymerases are halted by mechanical forces (a collective phenomenon that we call a polymeton). We also show that incorporating the impact of DNA twisting on both recruitment of RNA polymerase and their interaction can correctly predict observed fluctuations in gene expression. Finally, we use the mechanical coupling between polymerases to propose a computational model of a toggle switch whereby interactions between two genes are mediated by DNA twisting as opposed to proteins.

MATERIALS AND METHODS

Simulation details and parameters

Simulations were conducted in MATLAB. Euler's method was used for the numerical integration of the twist angles given in Eq. 7. Integration steps of size $\Delta T = 1/200(s)$ where used. The same method was applied for the integration of polymerase motion. See (15) for more details. Stochasticity for the initiation of polymerases, degradation of produced mRNA, and topoisomerase action were modeled as Poisson processes. This was implemented in the simulation by allowing for each process to occur within each time-step with a probability specified by the rate for that process.

RESULTS

Model description

Two major factors determine gene expression output. The first is the rate at which polymerases are recruited at the transcription start site, referred to as the initiation rate. Second is the rate at which the recruited polymerases are transported from the start site to the termination site, referred to as the elongation rate. The rates of initiation and elongation together determine the rate of gene expression output.

Fluctuations in the output are not necessarily equal to fluctuations created during initiation because polymerase velocity and spacing can change during transport. To understand the fluctuations in the output and how they relate to the fluctuations in the input, we need to model the transport of polymerases and quantify their contribution to the fluctuations in the output.

Our model describes the position and velocity of the polymerases during transport. We assume that there are N polymerases between the transcription start site and the termination site. The ith polymerase has position x_i and velocity v_i. The density function of the polymerases $\rho = \sum_i \delta(s - x_i(t))$ encodes the position of all the polymerases along the gene, where the position along the gene is parameterized by s (in bp). Similarly, the flux of polymerases along the gene is defined as

$$j(s,t) = \sum_i v_i(t)\delta(s - x_i(t)). \quad (1)$$

Flux j at position s corresponds to the number of polymerases crossing s per unit time. The unit of flux is the same as that of the initiation and output rates. The flux captures the transport of polymerases along the gene and can be used to link initiation and elongation to output (Fig. 1).

At steady state, the initiation rate is equal to the output rate when averaged over a sufficiently long period of time. In addition, these rates should equal the average flux at any point along the gene when there is no depletion of polymerases along the gene. However, the fluctuations in these three rates are not necessarily equal. To understand how variations in the flux control output fluctuations, we need to incorporate the physical factors that modify polymerase velocity and the initiation rate.

As polymerase moves along the gene, it can change the degree of supercoiling. This is because to transcribe, a polymerase has to either 1) rotate to follow the helical grooves of DNA and/or 2) DNA itself has to twist as it is pulled through a polymerase (8). Polymerase rotation does not change the degree of supercoiling, whereas DNA twisting does (23). Therefore, we need to incorporate the feedback between polymerase velocity and DNA supercoiling in our model.

Following a physical construction of the twin-domain model of transcription (23), we define $\dot{\theta}_i$ to be the rate of rotation (angular velocity) of the ith polymerase. $\varphi(s)$ is the twist of DNA at position s calculated from the molecular axis of DNA (32). We define $\varphi(s = 0) = 0$. Even with zero supercoiling, as s increases, φ also increases because of the natural helical form of DNA at a rate of $\omega_o = 0.6\,[rad/bp]$ (for relaxed DNA). $\dot{\varphi}(s)$ is the rate of twisting per unit time at position s. $\partial_s\varphi$ evaluated position s_0 captures how the degree of

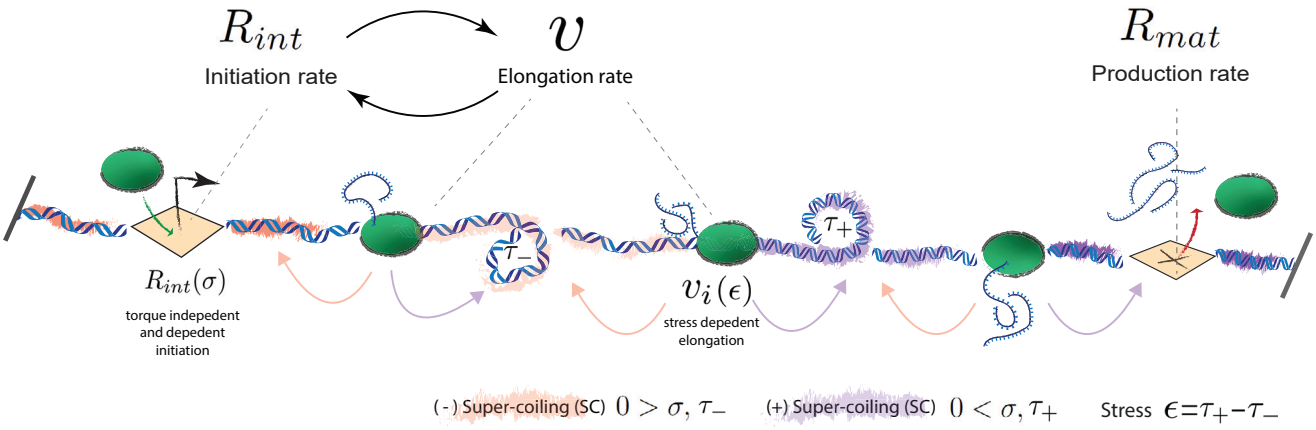

FIGURE 1 Schematic of the model of the role of supercoiling during transcription. Gene expression output is determined by both polymerase recruitment (initiation) as well as polymerase transport along the gene (elongation). During elongation, polymerases produce supercoiling, the over and under twisting of DNA (shown in *purple* and *red*, respectively), causing a corresponding change in the torque and in turn the torsional stress on the DNA. DNA supercoiling and torque can be transported between polymerases creating nonlocal interactions between polymerases that influence elongation and initiation. These interactions also impact both the average rate of mRNA production and its fluctuations. To see this figure in color, go online.

twist changes when moving along the gene from position s_0 to a point infinitesimally away $s_0 + ds$. $\partial_s\varphi$ is referred to as the local twist density.

Thus, $v\partial_s\varphi$ determines the rate at which a polymerase encounters twist when moving at velocity v along the gene. To follow the grooves of DNA, a combination of polymerase rotation or DNA twisting (in the opposite direction) must occur (23). Therefore, for the ith polymerase, the equation

$$v_i\partial_s\varphi(s,t) \;=\; \dot{\theta}_i(t) \;-\; \dot{\varphi}(s,t) \tag{2}$$

encodes the local interplay between DNA twist density encountered during elongation, polymerase rotation, and further DNA twisting.

Here, we will only consider changes in DNA supercoiling due to local DNA twisting, neglecting the role of writhe. The role and addition of DNA bending and writhe are discussed later. We define the local supercoiling density σ to be the normalized excess twist density in DNA. Mathematically, we express σ using the natural twist density (here defined as $\omega_0 \;=\; 0.6\;[rad\,/bp]$) as

$$\sigma(s,t) \;=\; \omega_o^{-1}\partial_s\varphi(s,t) \;-\; 1. \tag{3}$$

We can write Eq. 2 using the supercoiling density σ instead of the local twist density $\partial_s\varphi$.

$$v_i(t)(1+\sigma(t))\omega_o \;=\; \dot{\theta}_i(t) \;-\; \dot{\varphi}(s,t) \tag{4}$$

We can use mechanics to relate the rate of rotation of polymerase $\dot{\theta}_i$ and the rate of twisting of DNA $\dot{\varphi}(s)$ to the torque applied to the polymerase or DNA at position s. At each position s, there exists some amount of torque $\tau(s)$ in response to the amount of twisting $\varphi(s)$ at that position. The torsional stress $\epsilon_i(t) \;=\; \partial_s\tau(s = x_i, t)$ (also called the local torque per unit length) exerts a damping force on the polymerase that rotates it. Intuitively, torsional stress can be thought of as the difference of the torque in front of and behind the polymerase. Specifically, the rate of rotation of ith polymerase is given by

$$\big(\gamma + \eta x_i^{\alpha}(t)\big)\dot{\theta}_i(t) \;=\; \epsilon_i(t), \tag{5}$$

where the drag coefficient has a constant term γ and a term that increases with the distance x_i of the polymerase from the transcription start site. The drag coefficient increases with the distance of the polymerase from the start site because the nascent RNA attached to the polymerase increases in length as the polymerase moves along the gene. γ captures the drag of polymerase and DNA without nascent RNA attached. α is a phenomenological parameter that captures how the drag coefficient changes with the distance from the start site (33).

Similarly, the rate of rotation of DNA at position s away from transcription is related to the torsional stress experienced by the DNA at that position.

$$\zeta\dot{\varphi}(s,t) \;=\; \epsilon(s,t), \tag{6}$$

where ζ is the constant drag coefficient of DNA and $\epsilon(s,t) \;=\; \partial_s\tau(s,t)$.

By substituting Eq. 5 into Eq. 4 to eliminate $\dot{\theta}$, we obtain an equation for the rate of rotation of DNA at the position of the ith polymerase:

$$\dot{\varphi}_i(t) \;=\; -\,\omega_o(1+\sigma)v_i(t) + \epsilon_i(t)/(\gamma + \eta x_i(t)^{\alpha}). \tag{7}$$

This equation directly relates the dynamics of DNA twisting to the rate of polymerase elongation v_i and positioning x_i.

To write Eq. 7 for any position s on the gene, we combine the discrete drag coefficients of individual polymerases and the continuous drag coefficient of DNA and define

$$D(s,t) = \frac{1}{\omega_o \zeta}\left(1 - \sum_i \delta(s - x_i(t))\right) + \frac{1}{\omega_o}\sum_i \frac{\delta(s - x_i(t))}{\gamma + \eta x_i^{\alpha}(t)}. \quad (8)$$

Using the above form of the drag coefficient and our previous definition of flux j (Eq. 1), we can write down an equation for the dynamics of DNA twisting that combines the contribution of polymerases with that of DNA itself:

$$\dot{\varphi}(s,t) = -\omega_o(1+\sigma(s,t))j + \omega_o D(s,t)\epsilon(s). \quad (9)$$

By applying Eq. 3, we arrive at a supercoiling density transport equation for transcription:

$$\partial_t \sigma(s,t) = \partial_s(-(1+\sigma(s,t))j + D(s,t)\epsilon(s,t)). \quad (10)$$

This result stands in contrast to previous models (24,34), which assume a constant diffusion coefficient and neglect the fact that polymerases serve as both a source of supercoiling as well as barriers to its free diffusion (35).

We can write Eq. 10 explicitly in terms of σ (and thus stress) by specifying the local torque as

$$\tau(s,t) = C\sigma(s,t), \quad (11)$$

where C is the twist modulus of DNA ($75[nm] \times k_bT$ (36)). Here, we do not account for DNA bending or writhing in our simple model, though their analytical inclusion is straightforward (37–39). Their inclusion can lead to DNA buckling, resulting in altered twist transport and torsional responses. To account for buckling in our simulations, we will utilize a phenomenological relationship between torque and supercoiling (see supporting material).

The flux term in the above equation and the diffusion constant depend on the position and the velocity of the polymerases. To close the set of equations in our description, we need to relate the position of the polymerases to their velocity and relate their velocity to the supercoiling density σ. The position of the polymerase ith change in time as $\dot{x}_i = v_i$.

We assume a phenomenological relationship between the supercoiling density and the velocity of polymerase i using the following functional form:

$$v_i(t) = \frac{v_{max}}{1 + e^{\kappa(\epsilon_i(t) - \epsilon_c)}};\ \epsilon_i = \partial_s \tau(x_i), \quad (12)$$

where ϵ_i is the torsional stress experienced by the ith polymerase as previously defined. ϵ_c is the torsional stress cutoff (around 0.2 N for *E. coli* (28) assuming that the length scale of the polymerase is 0.6 Å (40)). v_{max} is the maximum velocity that polymerases can travel when $\epsilon_i << \epsilon_c$. Conversely, if $\epsilon_i >> \epsilon_c$, then the polymerase stalls. This phenomenological form is motivated by the empirical observations made in (28).

Taken together, Eqs. 10–12 provide a closed-form description of the generation and transport of supercoiling density along the gene due transcription as well as the position and velocity of each polymerase. To solve these equations, we need to also specify the initial conditions and the boundary conditions. $s = 0$ and $s = L$ are the positions of the two boundaries of the system. The boundaries of the gene itself (marked by the position of the transcription start site and termination site) are contained within the boundaries of the system. For an open system (DNA that is free to rotate at the boundaries), we have $\sigma(s = 0) = \sigma(s = L) = 0$. Similarly, for DNA that forms a closed loop, $\sigma(0) = \sigma(L)$, $\partial_s\sigma(0) = \partial_s\sigma(L)$ so that the supercoiling density and torques match at the beginning and end of the system but are not necessarily zero. In our simulations, we use fixed boundary conditions where the gradient of supercoiling density at the two boundaries is zero, $\partial_s\sigma(s = 0) = \partial_s\sigma(s = L) = 0$, at all times, but the supercoiling densities are not necessarily equal to each other, $\sigma(0) \neq \sigma(L)$.

The above equations with the boundary conditions specified can be simulated to study the generation and transport of supercoiling density along the gene. In our simulations, we assume the limit of fast diffusion of supercoiling density between the polymerases. This limit corresponds to $\zeta \to 0$ in Eq. 8. With this assumption, the supercoiling density is constant along DNA regions between polymerases, allowing us to directly use Eq. 7 to keep track of supercoiling in alignment with previous efforts (23).

Finally, we incorporate the role of topoisomerases into our simple model. Topoisomerases play an important role in regulating transcription in both bacteria and eukaryotes (41). General classes of topoisomerases are formed by their ability to relieve either positive or negative supercoiling density as well as their mechanisms of actions, which use either single- or double-strand breaks to modify the supercoiling density (42).

If no mechanism to relieve supercoiling is included (such as the one provided by topoisomerase), then large amounts of supercoiling density accumulate and stalling occurs for reasonable choices of parameters as observed in experiments (43). To incorporate topoisomerase action in our model, at random time points, we scale the supercoiling at every point along the gene by the same constant factor by reassigning the twist at each polymerase $\varphi_i \to a\varphi_i$ ($a = 0.1$ in our simulations; the value of this constant is not important because the rate of topoisomerase action is the free parameter in our simulations).

The rate at which topoisomerase acts is set by the difference of the supercoiling density at the two boundaries:

$$\Omega(t) = \sigma(L,t) - \sigma(0,t). \quad (13)$$

$\Omega(t)$ roughly corresponds to the accumulation of supercoiling density along the gene over time. In our simulations, we use the following form for the rate of topoisomerase action as a function of $\Omega(t)$:

$$R_{topo}(t) = \lambda \frac{1}{1+\Omega(t)}. \quad (14)$$

Thus, the overall rate of supercoiling density removal due to topoisomerase action goes as

$$\lambda \frac{\Omega(t)}{1+\Omega(t)}, \quad (15)$$

so that the rate of removal saturates with increasing levels of supercoiling at a fixed topoisomerase concentration. The above form is motivated by empirical observations of the dynamics of topoisomerase action in vitro (44). In these experiments, supercoiled plasmids were prepared at varying concentrations, effectively altering the amount of supercoiling present, Ω (44). Multiple types of topoisomerases were then added to remove the supercoiling. All topoisomerases displayed kinetic behavior in the form of Eq. 15. Thus, the phenomenological action of topoisomerase in our model closely captures the known kinetic properties of topoisomerases. As a check, we tried multiple alternative phenomenological forms relating $\Omega(t)$ to the rate of topoisomerase action: a constant rate independent of $\Omega(t)$, a rate proportional to $\Omega(t)$, and a rate that approaches zero with increasing $\Omega(t)$. The form used in Eq. 15 was the only one that was consistent with empirical observations of how topoisomerases regulate polymerase velocities and fluctuations in mRNA production (see supporting material).

Simulations

We simulated the model described above to understand how initiation, transport, and supercoiling work together to determine gene expression output (the simulations are described in detail in the supporting material). To do this, we simulated a single isolated gene of length 1,000 bp contained within a total stretch of DNA of length (L) = 3,000 bp. The start site of the gene is located at s = 1,000 bp. At $s = 0$ and $s = L$, DNA will be prevented from freely rotating, causing supercoiling density to build up at the boundaries corresponding to the fixed boundary condition.

We begin with a constant initiation rate that does not depend on the supercoiling density at the transcription start site. Therefore, the loading process of polymerases at the transcription start site (s = 1,000 bp) is a Poisson process with rate R_{int}. We will later consider an initiation rate that is a function of the supercoiling density at the transcription start site.

As the polymerases move along the gene, the supercoiling density changes according to Eq. 7, which governs the local twist change at each transcription site. We set the drag coefficient $\gamma = 10^{-1}$[pNs] and the phenomenological parameters $\eta = 10^{-4}$[pNs /bp^2] and $\alpha = 2$. While there is little empirical data to determine the precise values of these parameters, biophysical considerations (as well as the observation that short genes do not induce supercoiling while long ones do (35)) implies a drag greater than 1 pNnm for a nascent transcript of length 1 kbp or greater rotating at 10 *rad/s*. We will, regardless, show that our results are robust to changes in the values of these parameters (see results and discussion and supporting material). We assume that the torque is related to the supercoiling density using the functional form shown in the supporting material. This choice is motivated by empirical observations (36) and only contains one free parameter, which sets the torque at which DNA buckles. We also ensured that our results are robust to the choice of this parameter (see Fig. S1).

When a polymerase reaches the transcription termination site, a mature mRNA is produced that then is removed at a constant rate $\mu = 10^{-2}s^{-1}$. The simulations were started with no polymerases on the gene and ran for a sufficiently long period of time to reach steady state when the number of RNA polymerases stabilized. We observed that the simulations reached steady state typically after 10 min out of a total of 1 h of simulation time (timescale set by μ).

Fig. 2 *a* shows a snapshot of the simulation with three polymerases moving along the gene. For each simulation run, we computed the number of mRNA molecules averaged across multiple simulation samples after each simulation reached steady state. The average number of mRNA is plotted as a function of the initiation R_{int} for different values of parameters λ and v_{max} (Fig. 2 *b*). As expected, the number of mRNA molecules is proportional to R_{int} but does not depend on the values of λ and v_{max}. This is because at steady state, the rate at which polymerases are loaded must equal to the rate of production of mRNA.

The average velocity at which the polymerases move along the gene (shown in Fig. 2 *c*) also depends on R_{int} but saturates to a value that does not necessarily correspond to v_{max}, especially when the rate of topoisomerase action λ is low or the ends of DNA are free. Importantly, this behavior recapitulates three empirical observations. One is that the polymerase velocity changes as the rate of topoisomerase action changes (4,25). Second is that the velocity of polymerases can be smaller than the bare velocity (v_{max}/2), defined as the velocity of a single polymerase moving along a linear piece of DNA with open boundaries where there is no accumulation of supercoiling density (4,25). Third, actively elongating polymerases can be slowed by turning off further polymerase initiation (4) (Fig. S3).

To gain an intuition for this behavior, consider the simplest case where all the polymerase velocities are equal to v. In addition, we assume that there is sufficiently large drag

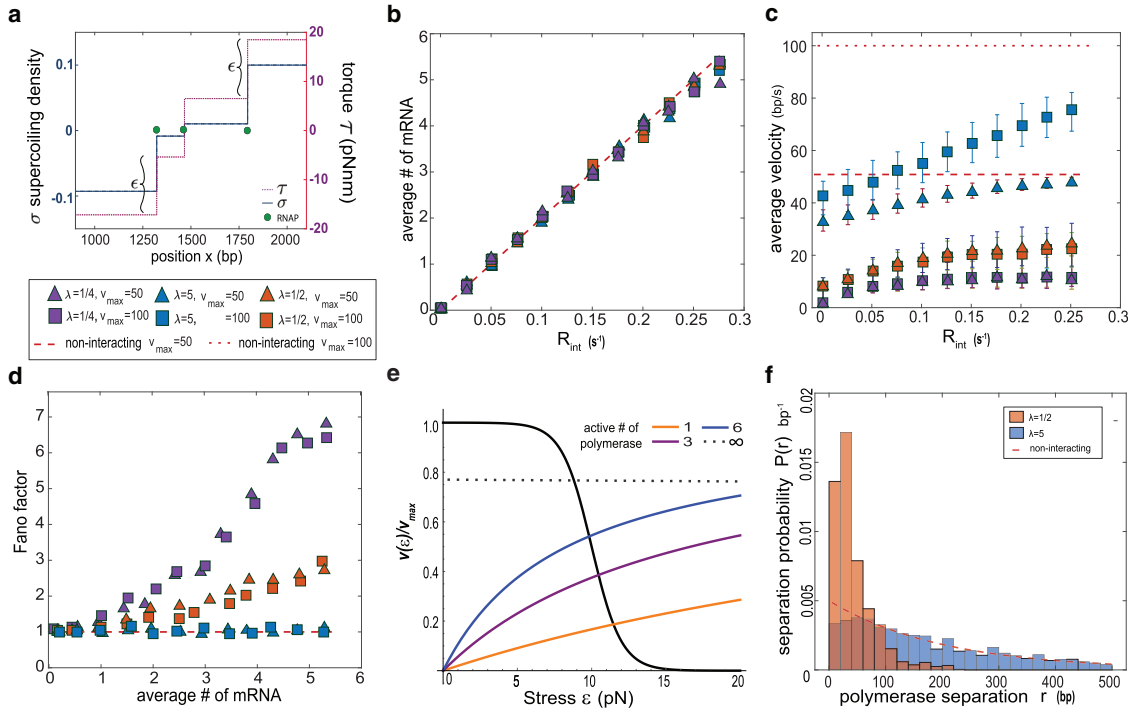

FIGURE 2 DNA supercoiling-mediated interactions between polymerases do not alter the average mRNA production rate but link polymerase clustering to mRNA bursting. (*a*)Transcribing polymerases generate supercoiling density σ and accompanying torque during elongation. (*b*)The average number of mRNAs produced is insensitive to the elongation kinetics of the polymerases and is solely determined by the initiation rate. Changing the elongation kinetics by altering the maximum polymerase elongation rate v_{max} or the rate of topoisomerase action λ does not change the production rate. (*c*) Average elongation rates depend on the initiation rates and therefore the average number of polymerases present on the gene, demonstrating a cooperative interaction between the polymerases. The elongation rate plateaus to a value that is predominantly set by the rate of topoisomerase action. Error bars indiate the standard deviation. (*d*) A monotonic relationship between the mean mRNA production rate and its fluctuations (Fano factor) emerges with the slope determined by the rate of topoisomerase action. A high rate of topoisomerase action results in fluctuations that resemble the Poisson statistics of noninteracting polymerases (*red dashed line*). (*e*) Analytical expressions for the elongation rate (*black* given by Eq. 12) and the rate of topoisomerase action (*colors and dotted* given by Eq. 15) as a function of the stress. The steady-state value of stress set when the rate of addition of supercoiling equals the rate of its removal (Eq. 17), shown as the intersection of the black and colored curves. The value of stress at this interaction thus determines the elongation rate according to Eq. 12. (*f*) Supercoiling-mediated interactions change interpolymerase separation distances. The separation distance between the polymerase nearest the transcription start site and its closest neighbor, *r*, decreases with increasing accumulation rate of supercoiling density. The altered separation distances result in higher fluctuations in gene expression. The distribution of separation distances deviates from that of noninteracting polymerases that follow Poisson statistics (exponentially distributed separation distances, shown by *red line*). Simulation details are described in the supporting material. To see this figure in color, go online.

$(\gamma + \eta x^{\alpha} >> 1)$ on each polymerase so that we can ignore polymerase rotation $(\dot{\theta} = 0)$. In this case, the supercoiling density generated by each polymerase is canceled by the supercoiling density generated by the neighboring polymerases except for at the boundaries where there is no cancellation. Then, the rate of supercoiling density generation is $-\omega_o v$ at the boundary closest to the start site and $\omega_o v$ at the other boundary (Eq. 10). Therefore, we can write an equation for the rate of change Ω (Eq. 13) as

$$\dot{\Omega} = 2\omega_o v - \lambda \frac{\Omega}{1+\Omega}, \tag{16}$$

where the second term on the right-hand side is the rate of removal of supercoiling density by topoisomerase action. At steady state, $\dot{\Omega} = 0$.

If we make the additional simplifying assumption that the change in supercoiling density across each polymerase is proportional to the torsional stress on that polymerase ϵ (i.e., ignoring DNA buckling), then $\Omega = N\epsilon$, and Eq. 16 can be written as a function of N and ϵ as

$$Cv(\epsilon) - \lambda \frac{N\epsilon}{1+N\epsilon} = 0. \tag{17}$$

The above equation sets the value of torsional stress ϵ for each polymerase and, in turn, their velocity. Fig. 2 *e* shows the contribution of each term in Eq. 17 as a function of ϵ.

Increasing the polymerase loading rate R_{int} increases N. However, the rate of removal of supercoiling density due to topoisomerase actions saturates with increasing N (Fig. 2 *e*). The value at which this saturation occurs sets the value of torsional stress on each polymerase and thereby their average velocity. The dashed curve shows the smallest possible ϵ that satisfies Eq. 17 when $N \to \infty$ and in turn sets the values of elongation rate for large R_{int} in Fig. 2 *c*.

Because of the saturation of the rate of topoisomerase action, the average polymerase velocity can be smaller than the maximum allowed velocity v_{max}. Other choices for the functional form relating the rate of topoisomerase action to $\Omega(t)$ such as $R_{topo} \sim Cnst.$ or $R_{topo} \sim \Omega(t)$ will not result in a velocity that saturates to a value other than v_{max} for large N, in disagreement with empirical observations where average polymerase elongation velocities both plateau as a function of initiation rate but do so at a value less than v_{max} (4,25).

Next, we computed the fluctuations in the number of mRNA molecules. We computed the Fano factor of the number of mRNA molecules (variance divided by mean) over the entire duration of the simulation after steady state was reached. Surprisingly, the Fano factor deviates from simple Poisson statistics at a sufficiently high initiation rate and a low rate of topoisomerase action (Fig. 2 *d*). This is because as polymerases move along the gene, they interact with each other and change their separation distances (referred to as clustering) from the initial exponentially distributed separation distances set by the Poisson loading process (Fig. 2 *f*). With interactions, the distribution of separation distances peaks at a nonzero value and has a narrower range, as evident in Fig. 2 *f*. This effect is larger for a lower rate of topoisomerase action because the interactions are mediated by the accumulation of supercoiling density. Clustering of polymerases due to interactions is a plausible explanation for the universally observed "bursting" dynamics of gene expression and the relationship between the average number of transcripts observed in individual cells and the fluctuations of the number of transcripts across cells in a population (11). The model shows a qualitative relationship between average polymerase velocity and fluctuations in mRNA production (Fano factor, i.e., bursting), consistent with experimental observations. In these experiments, decreasing the rates of topoisomerase action (λ in our model) leads to a decrease in the average polymerase velocities and an increase in the levels of mRNA fluctuations (see Figs. 3 and 7 in (25)). The same behavior is also displayed by our model (Fig. 2 *c* and *d*). Additionally, previous experiments have shown that fluctuations in mRNA production (bursting) are linked to polymerase separation ("clustering") (26,27) by directly observing polymerases as they elongate. Our model is the first theoretical demonstration of this link (Fig. 2 *d* and *f*).

To gain an intuition for how clustering occurs, consider the dynamics of two neighboring polymerases. The relative distance between the two polymerases changes as

$$\dot{r} = v_1(\epsilon_1) - v_2(\epsilon_2), \tag{18}$$

where the velocity of each polymerase is determined by Eq. 12. The torsional stress experienced by the first and second polymerase is a function of supercoiling density in front of, in between, and behind the two polymerases' σ_F, σ_M, and σ_B, respectively. In particular, $\epsilon_1 \propto \sigma_F - \sigma_M$ and $\epsilon_2 \propto \sigma_M - \sigma_B$. Because supercoiling density always accumulates in the front and all polymerases move in the same direction, $\sigma_F > \sigma_M > \sigma_B$. Importantly, the supercoiling density between the two polymerases is inversely proportional to their separation distance, $\sigma_m \propto 1/r$. If the separation distance between two polymerases is large, then σ_m is small, which in turn generally implies $\epsilon_1 > \epsilon_2$ and $v_1 < v_2$. Therefore, in the case of large separation, $\dot{r} < 0$, and the separation distance between the two polymerases shrinks. Conversely, if the separation distance between the two polymerases is small, then σ_m is large, which in turn generally implies $\epsilon_1 < \epsilon_2$ and $v_1 > v_2$ and an increasing separation distance $\dot{r} > 0$. Taken together, as polymerases move along the gene, because of the interactions, they converge to a preferred separation distance (Fig. 2 *f*) and then move with a constant velocity (Fig. 3 *b*). This is the first theoretical description of a natural mechanism for polymerase clustering (26,27).

Surprisingly, in our simulations, we observed that a minimum number of three interacting polymerases moves a larger distance before stalling compared with one or two polymerases, as shown in Fig. 3 *b*. To gain an intuition for why a minimum of three interacting polymerases are required for sustained motion, consider how stress accumulates as one polymerase moves along the gene. We can write an equation for the rate of change of the velocity of the polymerase $\dot{v}$ in terms of the dynamics of the local stress by applying a simple chain rule to the stress-dependent velocity (Eq. 12):

$$\dot{v}_i(\epsilon_i) = \frac{d}{d\epsilon_i} v_i(\epsilon_i)\dot{\epsilon}. \tag{19}$$

An isolated polymerase moves at velocity v_{max} initially. As it moves along the gene, the torsional stress across the polymerase accumulates at a rate that is proportional to its velocity, $\dot{\epsilon} \propto v$. Substituting this into Eq. 19 implies $\dot{v} \propto -v$. Therefore, the velocity of the polymerase decays exponentially to zero. When topoisomerase relieves the stress, the polymerase can start to move again. When two polymerases move along the gene, their velocities converge to the same value as described above. As with the case of an isolated polymerase, the two polymerases also accumulate torsional stress at a rate proportional to their velocity. This occurs even though supercoiling does not accumulate in the region between the two polymerases because the negative supercoiling density generated by the leading polymerase cancels the positive supercoiling density generated by the trailing polymerase. However, supercoiling density does accumulate outside the two polymerases because there is no cancellation. Therefore, the velocities of the two polymerases also decay exponentially, as is the case with a single polymerase (shown in example traces in Fig. 3 *b*).

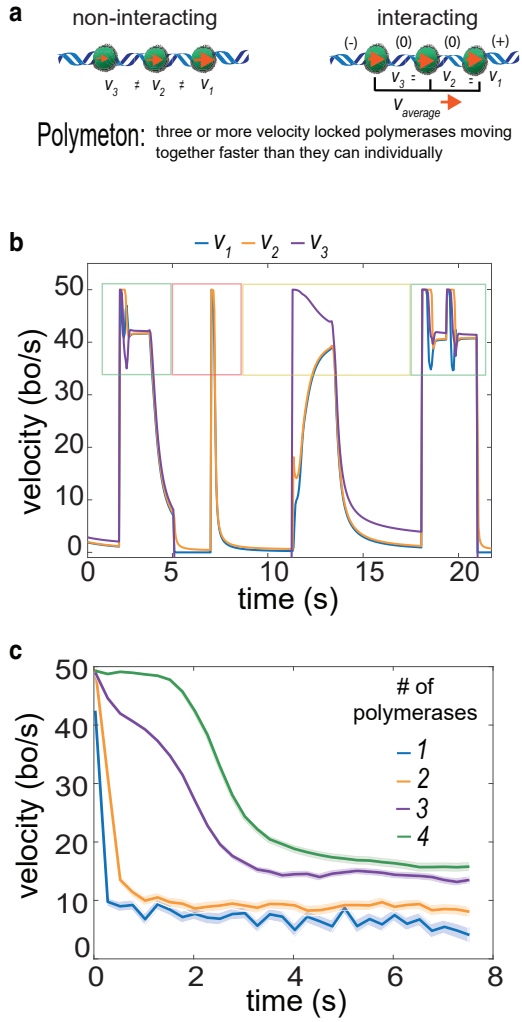

FIGURE 3 Supercoiling-mediated interactions lead to cooperative elongation rates through the creation of polymetons. (*a*) Supercoiling density differences across different polymerases lead to velocity differences that in turn change the polymerase separation distances. Polymetons are velocity-locked groups of three or more polymerases where supercoiling density does not accumulate for the middle polymerase. (*b*) Representative velocity trajectories that show cycles of elongation and stalling due to supercoiling density accumulation and release via topoisomerase action. Three polymerases moving as a polymeton are initially present on the gene labeled with numbers that increase from the termination site to the start site (*green square*). At approximately t = 5 s, the leading polymerase reaches the termination site and is removed, leaving behind two polymerases that rapidly stall (*orange square*). Initiation of a new polymerase at the start site increases the elongation rate of the two stalled polymerases mediated through supercoiling-induced interactions (*yellow square*). Finally, the three polymerases again form a polymeton and elongate with approximately similar velocities (*green square* on the right). (*c*) The average elongation rate as a function time following topoisomerase action binned by the number polymerases present on the gene. There is a clear jump when the number of polymerases present changes from two to three, showing the formation of polymetons. To see this figure in color, go online.

This picture changes qualitatively with the addition of a third polymerase. The velocities of the three polymerases also converge to a shared constant value as they move along the gene. However, the supercoiling density generated by the middle polymerases is exactly canceled by the two polymerases on either side. Therefore, the middle polymerase has no torsional stress accumulation. This puts the middle polymerase in a privileged position. As the outer two polymerases slow down from the accumulation of stress, the middle polymerase continues to move. When this happens, the middle polymerase accumulates torsional stress because there is no exact cancellation of supercoiling density from the other two polymerases. Importantly, the accumulation of supercoiling density in the middle relieves torsional stress on the outer polymerases, resulting in their collective motion. Taken together, three polymerases can sustain their motion for significantly longer periods of time before stalling (as shown in the traces in Fig. 3 *b*).

In summary, our results show that there is an emergent phenomenon where three or more polymerases can sustain their collective motions for a longer period of time than one or two polymerases. We will refer to three or more interacting polymerases undergoing sustained motion as polymetons. Polymetons emerge in our system following a topoisomerase action when three or more simultaneously elongating polymerases move at near-constant velocity (Fig. 3 *b*). The simplified discussion of the behavior of a polymeton above discounts the fact that polymerases in a polymeton are at different positions along the gene and therefore are attached to nascent RNAs of different lengths. The model used in our simulations accounts for this subtle difference, which breaks the strict symmetry discussed above, leading to differences between three and four polymerases in a polymeton, as seen in Fig. 3 *c*. However, the qualitative behavior that middle polymerases occupy a privileged position and can assist in sustaining the motion of the group should not depend on the precise form of the model.

Torque-dependent initiation

Next, we incorporate torque-dependent initiation into the model. Up to this point, polymerase initiation in the model occurs stochastically as a Poisson process with a constant rate R_{ini}. However, there is experimental evidence that the initiation rate should depend on the supercoiling density at the promoter site. First, there are in vivo measurements showing that increasing the level of negative supercoiling at a promoter by inducing the production of neighboring genes can alter its output (5,31,45,46). Second, in vitro single-molecule experiments have directly measured promoter-unwinding kinetics as a function of the torque in DNA (40), demonstrating that initiation is sensitive to the torque at the promoter.

Polymerase initiation is basically an ordered process of polymerase binding to DNA at the promoter site, unwinding of the DNA, and polymerase leaving the promoter (referred to as clearance). Polymerase-DNA binding follows standard

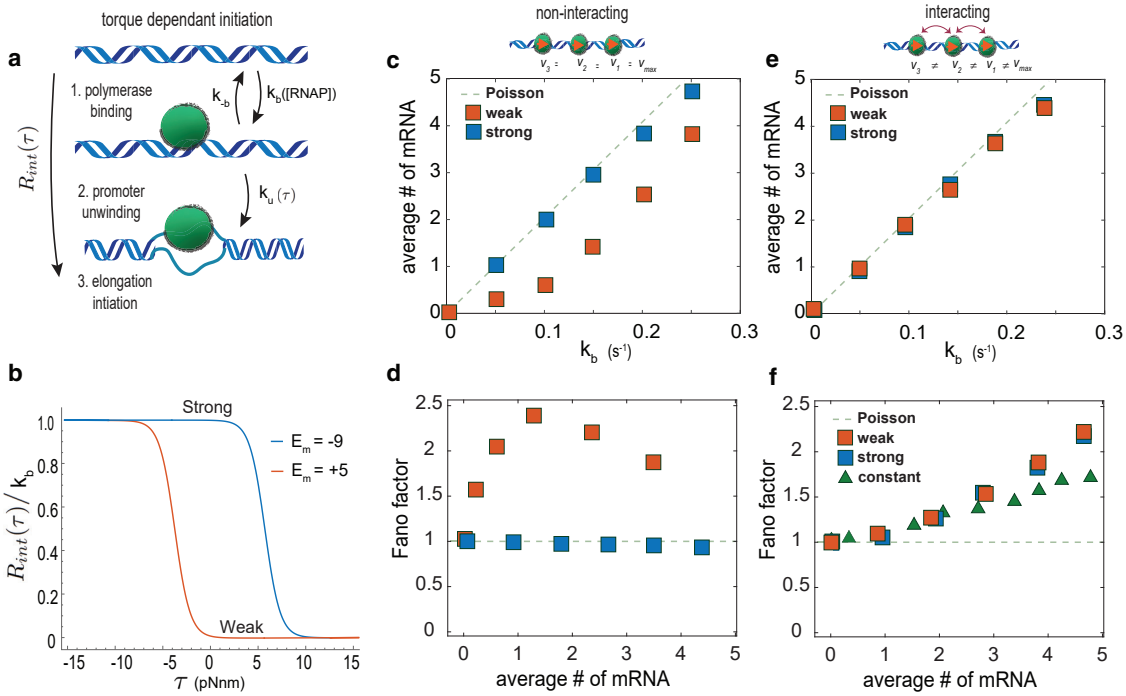

FIGURE 4 Torque-dependent initiation alongside supercoiling mediated interactions recapitulates the expected mean mRNA production rate and its fluctuations. (*a*) Torque-dependent initiation is a two-step process: a reversible polymerase binding step that does not depend on torque but on the free RNA polymerase concentration, followed by an irreversible promoter unwinding step which depends on the torque at the promoter site. (*b*) A weak promoter ($E_b > 0$) is more sensitive to the torque at the promoter site than a strong promoter ($E_b < 0$) requiring negative torque to initiate transcription. (*c* and *d*) Mean expression and expression fluctuations (Fano factor) for torque-dependent initiation with increasing polymerase binding rate k_b both in the absence of supercoiling mediated interactions between polymerases. The weak promoter exhibits a production rate that scales nonlinearly with k_b (*c*) and nonmonotonic fluctuations in expression (*d*). (*e* and *f*) Same as in (*c* and *d*) but with the addition of supercoiling mediated interactions between the polymerases. Both strong and weak promoters exhibit linear production rates in k_b (*e*) with fluctuations that increase monotonically with the average production rate (*e*). The green triangles in (*f*) show the fluctuations when interactions are present but the initiation is a torque-independent Poisson process (as in Fig. 2). To see this figure in color, go online.

chemical kinetics whereby the binding rate increases proportionally with polymerase concentration and promoter affinity, K_o, which captures the intrinsic affinity of polymerase for the promoter, $k_b = [RNAP]K_o$. The unbinding rate of polymerase from the promoter, k_{-b}, is not sensitive to polymerase concentration (47). Precise kinetic observations (40,47) have measured these rates for specific promoters and could thus be used as inputs into a model of initiation. In our model, we explicitly vary k_b to capture the behavior of genes with different promoter affinities and polymerase concentrations. Inducing or repressing a gene corresponds to varying k_b.

Following promoter binding, the polymerase locally unwinds the DNA at the promoter site. This step has a strong dependence on the torsional state of DNA and can become the rate-limiting step in initiation. Precise characterization of promoter unwinding and clearance by polymerases for varying levels of DNA supercoiling has been made (40). The rate of unwinding depends on the level of torque at the promoter site: the rate of unwinding decreases as torque is increased following a simple Arrhenius law form as measured by (40). Consequently, we model the unwinding rate k_u as

$$k_u = e^{-\left(\tau_{prom}(t)\delta + E_m\right)}. \tag{20}$$

δ captures the dependence of the unwinding rate on the torque τ. E_m captures the strength of the promoter and can vary from one promoter to another. E_m sets the value at which torque unwinds specific promoters and allows transcription. Some promoters require negative torque to unwind and allow transcription (referred to as weak promoters), whereas strong (consensus) promoters can unwind for positive values of torque (40) (rrnBP1 and lacCONS promoters, respectively).

Importantly, the torque at the promoter site, $\tau_{prom}(t)$, is given by the supercoiling density, which is in turn set by the polymerases as they move along the gene and interact (Eq. 10). Promoter clearance occurs rapidly following the promoter unwinding (47) and thus is ignored here. Collectively, our model of initiation is composed of a two-step process of reversible polymerase-DNA binding followed by irreversible promoter unwinding, which results in initiation (Fig. 4 *a*). Here, we utilize kinetic unwinding data of the Lac promoter (40) to model a strong promoter requiring no free parameters (see Fig. 4 *b*). The inferred values are $E_m = -9$

and $\delta = 2$ (values for $k_{\pm b}$ are given in (40)). The values for the weak promoter rrnBP1 are the same but with $E_m = 5$. This allows us to make a direct comparison between torsion-dependent initiation and gene expression for the same promoter (12) from experiments.

The torque-dependent initiation rate constructed above can be incorporated into our existing framework (Fig. 4). We first examine the role of torque-dependent initiation on gene output without polymerase interaction. Fig. 4 *c* and *d* show that a strong promoter is not affected by the changes in torque at the promoter site generated by the elongating polymerases even if they are not interacting. In this case, the gene mRNA output increases with the binding rate k_b but exhibits Poisson fluctuations (Fano factor = 1). A weak promoter (Fig. 4 *e* and *f*) displays a nonlinear relationship between the average mRNA output and the binding rate k_b. However, the fluctuations in the output display a nonmonotonic dependence on the mean expression, in disagreement with general experimental observations (11) as well as specific observations for the rrnBP1 and lac promoters (12).

Importantly, when the polymerases are allowed to interact as they move along the gene, the dependence of mRNA output and its fluctuation change. Both weak and strong promoters show a linear dependence of average mRNA output and binding rate k_b (Fig. 4 *e*). This output matches what would be expected if polymerase initiation did not depend on the torque but followed a simple Poisson process. The change in the behavior of output is because the torque at the promoter site changes when polymerases interact with each other. In addition, interacting polymerases also change how the mRNA output fluctuates (Fig. 4 *f*). Both weak and strong promoters now show super-Poissonian fluctuations with Fano factors that monotonically increase with the average output, again consistent with empirical observations of a super-Poissonian relationship between mean mRNA expression and mRNA fluctuations (see Fig. 3 of (12)).

Taken together, these results indicate that torque-dependent initiation alone is insufficient to explain the expected bursting behavior of genes. However, incorporating polymerase (velocity) interactions recovers the expected bursting behavior in genes pointing to fluctuations incurred during elongation as the overriding source of bursting in gene expression. Additionally, the insensitivity of strong promoters to negative torque (supercoiling) (40) calls into question the widespread use of initiation as the source of transcriptional bursting used in models (5,24,34).

Finally, the interplay between torque-dependent initiation and elongation could be exploited to engineer novel gene regulatory mechanisms or identify existing ones. For instance, imagine two identical genes convergently oriented toward one another both with weak promoters (Fig. 5 *a*). The gene that spontaneously initiates transcription first generates positive supercoiling density at the promoter site of the other gene because of the geometry of their arrangement. This supercoiling density in turn changes the initiation rate of the other gene. Therefore, the two genes repress each other resulting in DNA supercoiling-mediated toggle switch.

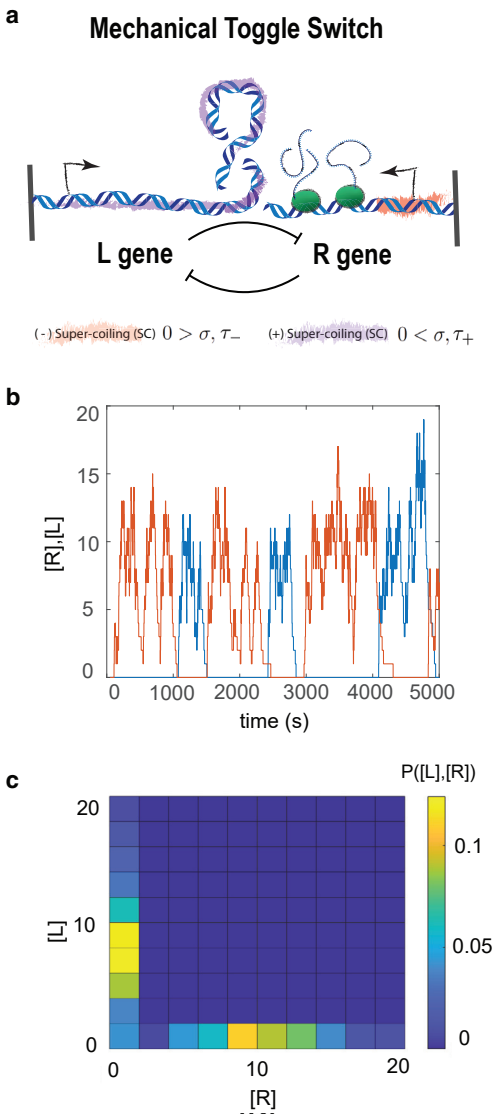

FIGURE 5 Mechanical toggle switch demonstrates that DNA supercoiling can be used to engineer interactions across genes without using proteins. (*a*) Two neighboring genes with their promoters oriented toward each other can regulate each other's expression through supercoiling-mediated initiation and elongation, resulting in a mechanical toggle switch. (*b*) Simulated production levels of two identical genes with weak promoters with the orientation shown in (*a*) as a function of time. The two genes mutually repress one another, leading to alternating periods of mRNA production by the [L] and [R] genes. (*c*) Alternating periods of mRNA production leads to a bimodal distribution of mRNA expression levels. To see this figure in color, go online.

To demonstrate this effect, we constructed a system of two convergently oriented, identical genes with torque-dependent initiation and weak promoters. Recent work has

examined a similar system (48). This system demonstrates bistable expression where when one gene is on, the other is off (Fig. 5 *b* and *c*). Importantly, the bistability of this system is not set by proteins, and therefore the timescale of the oscillations is independent of protein lifetimes. Elongating polymerases generate negative supercoiling at the on gene's promoter. Conversely, the elongating polymerases generate positive supercoiling at the off gene's promoter, resulting in continued repression of the off gene. Thus, the switching rate between states in a mechanical toggle switch is set by the average time a gene contains actively transcribing polymerases after initiation. For a switching event to occur, no new polymerases can initiate while there are actively elongating polymerases. This occurs with probability $e^{-r_{int}\overline{v}G_l}$, where $\overline{v}$ is the average polymerase velocity, G_l is the length of the gene, and r_{int} is the rate of initiation of new polymerase. Thus, the length of the gene has strong role in determining the switching time; longer genes create more stable states (see Figs. S4 and S5). Additionally, if either promoter is strong compared with the other promoter, or if polymerase loading is too slow, sustained toggling is not possible (Fig. S4). This simple system highlights the potential of novel forms of gene regulation mediated through supercoiling.

DISCUSSION

The framework introduced here provides a description of the supercoiling density generated during polymerase elongation, the transportation and accumulation of supercoiling density, and its resulting nonlocal effect on the elongation of polymerases. In addition, we introduced a mechanical model of transcription initiation compatible with our model of elongation. This addition is based on biophysical reasoning and in vitro observations of torque-dependent polymerase binding and is a crucial element in the construction of a comprehensive framework of supercoiling and transcription. Previous attempts have fallen short of a comprehensive description relying on discrete descriptions of polymerases(23), incomplete models of supercoiling transport due to elongation (24,34), or models that did not include both torque-dependent initiation (23) and elongation (24,34).

To make the model more computationally tractable, some simplifying assumptions were made. First, we assume that supercoiling density diffuses infinitely fast along the gene. This assumption was motivated because the mechanical state of DNA can relax much more quickly compared with the rate at which polymerase moves along DNA. Second, the conversion of DNA twist into writhe (bending) was not explicitly incorporated into our model. Consequentially, an explicit simulation of DNA twist transport alone would inadequately capture the mechanical response of DNA to twisting. Instead, we used a phenomenological formulation of the relationship between supercoiling density and torque, which implicitly includes DNA buckling (36). Similarly, a simple phenomenological framework was used to model the drag on elongating polymerases (33). Both of these phenomenological models are motivated by physical models of how polymers behave (33,36). Third, we constructed a simple model of topoisomerase action. Our model was motivated by empirical observations of topoisomerase kinetics acting on supercoiled DNA plasmids (44). The phenomenological form used in our model follows exactly the observations made in (44). Additionally, alternative forms resulted in behaviors that disagreed qualitatively with experimental observations (Fig. S2). Finally, the existence of cooperative elongation kinetics and polymetons was found to be robust under various phenomenological parameters used for DNA buckling, nascent mRNA drag, and topoisomerase action (Fig. S1).

The twist transport equation developed here (Eq. 9) can be used in future work to directly simulate the diffusion of twist in DNA during transcription. Recent theoretical work (49) has demonstrated that bursting can emerge with explicit supercoiling diffusion. Additionally, DNA writhing can be computationally or analytically incorporated, allowing for important effects such as histone occupancy dynamics to be included, which would make the model more suited to study chromatin dynamics. However, whether or not polymerase velocity (28) responds fast enough to fluctuating DNA stresses to form polymetons in real systems is left to be seen in experiments. Additionally, future work to connect model predictions of under and over twist to ensemble measurements (50) should be done.

Many model outcomes have been tested directly or are testable in future experiments. First is the observation that the rate of topoisomerase action determines the average elongation velocity of polymerases. It has been shown previously that the average elongation velocity is below the maximum elongation velocities of polymerases because of topoisomerase action (4,25). Additionally, it was previously shown that stopping initiation can slow already elongating polymerases (4). Our model correctly displays these same behaviors (Figs. 2 *c* and *e* and S3). The second observation is that the rate of topoisomerase action can control fluctuations in gene expression. Specifically, lowering the rate of topoisomerase action simultaneously lowers the average elongation velocity of polymerases while increasing fluctuations in mRNA production (Figs. 3 and 7 in (25)). Our model shows the same behavior (Fig. 2 *c* and *d*). The third observation is a super-Poissonian and monotonic relationship between the mean and the fluctuations in the number of mRNAs (see (11) and Fig. 3 in (12)). The model correctly predicts these three observations and links them all to the nonlocal interactions between polymerases mediated by supercoiling. We also predict that the extent of fluctuations in mRNA production is predominantly set by torque-dependent elongation as opposed to initiation (Fig. 4). This prediction can be tested by using reporters for directly

observing mRNAs as they are being transcribed (26,51) where one reporter is close to the promoter site while the other reporter is close to the end of the gene. The signals from the two reporters can be used to infer the extent of fluctuations generated by initiation versus elongation. A single reporter system of this kind has been previously used to confirm the relationship between bursting and clustering (26,27). Finally, similar reporter systems can be used to directly observe the formation of polymetons.

In summary, we show that nonlocal interactions between polymerases emerge from DNA supercoiling and lead to cooperative elongation rates, clustering of polymerases, and gene expression bursting, consistent with empirical observations of cooperative elongation kinetics (4), bursting (11), and clustering (26,27). This is the first theoretical effort to link bursting, clustering, and elongation rates together in a consistent framework with explicit mechanical interactions between polymerases. A collective phenomenon, referred to as polymetons, emerges whereby groups of three or more polymerases can sustain their elongation due to the privileged status of the interior polymerase. The addition of torque-dependent initiation alone is insufficient to reproduce observed relationships between the mean levels and fluctuations in gene expression. We found that including both torque-dependent initiation and elongation is sufficient to match experimental observations. This result calls into question the validity of using models of torque-dependent initiation alone that do not also incorporate interactions to explain gene expression fluctuations. Finally, we constructed an example where supercoilng can be used to build novel synthetic regulatory circuits using two neighboring genes to form a mechanical toggle switch.

In conclusion, we have shown that DNA supercoiling serves as a powerful mediating force between polymerases by altering initiation and elongation kinetics. These effects are inescapable physical attributes of transcription and offer a widespread nonlocal feedback mechanism between polymerases. This framework challenges the traditional decoupling of transcription initiation and elongation and has strong implications for models of gene expression fluctuations (52). Understanding the role that DNA mechanics plays in gene expression can provide new insights into how genes are regulated and will be essential in building future synthetic systems.

SUPPORTING MATERIAL

Supporting material can be found online at https://doi.org/10.1016/j.bpj.2022.09.026.

AUTHOR CONTRIBUTIONS

S.A.S. designed research, performed research, and wrote the paper; S.H. designed research and wrote the paper.

ACKNOWLEDGMENTS

The authors acknowledge funding from NIH NHLBI R01HL158269 grant.

DECLARATION OF INTERESTS

The authors declare no competing interests.

REFERENCES

1. Lenstra, T. L., J. Rodriguez, …, D. R. Larson. 2016. Transcription dynamics in living cells. *Annu. Rev. Biophys.* 45:25–47.
2. Le, T. B. K., M. V. Imakaev, …, M. T. Laub. 2013. High-resolution mapping of the spatial organization of a bacterial chromosome. *Science.* 342:731–734.
3. Marinov, G. K., A. E. Trevino, …, W. J. Greenleaf. 2021. Transcription-dependent domain-scale three-dimensional genome organization in the dinoflagellate breviolum minutum. *Nat. Genet.* 53:613–617.
4. Kim, S., B. Beltran, …, C. Jacobs-Wagner. 2019. Long-distance cooperative and antagonistic RNA polymerase dynamics via DNA supercoiling. *Cell.* 179:106–119.e16.
5. El Houdaigui, B., R. Forquet, …, S. Meyer. 2019. Bacterial genome architecture shapes global transcriptional regulation by DNA supercoiling. *Nucleic Acids Res.* 47:5648–5657.
6. Johnstone, C. P., N. B. Wang, …, K. E. Galloway. 2020. Understanding and engineering chromatin as a dynamical system across length and timescales. *Cell Syst.* 11:424–448.
7. Mirkin, S. M. 2001. DNA Topology: Fundamentals. John Wiley and Sons, Ltd.
8. Liu, L. F., and J. C. Wang. 1987. Supercoiling of the dna template during transcription. *Proc. Natl. Acad. Sci. USA.* 84:7024–7027.
9. Golding, I., J. Paulsson, …, E. C. Cox. 2005. Real-time kinetics of gene activity in individual bacteria. *Cell.* 123:1025–1036.
10. Raj, A., and A. van Oudenaarden. Oct. 2008. Nature, nurture, or chance: stochastic gene expression and its consequences. *Cell.* 135:216–226.
11. Sanchez, A., and I. Golding. 2013. Genetic determinants and cellular constraints in noisy gene expression. *Science.* 342:1188–1193.
12. So, L.-h., A. Ghosh, …, I. Golding. June 2011. General properties of transcriptional time series in Escherichia coli. *Nat. Genet.* 43:554–560.
13. Dar, R. D., B. S. Razooky, …, L. S. Weinberger. 2012. Transcriptional burst frequency and burst size are equally modulated across the human genome. *Proc. Natl. Acad. Sci. USA.* 109:17454–17459.
14. Larson, D. R., D. Zenklusen, …, R. H. Singer. 2011. Real-time observation of transcription initiation and elongation on an endogenous yeast gene. *Science.* 332:475–478.
15. Epshtein, V., and E. Nudler. 2003. Cooperation between rna polymerase molecules in transcription elongation. *Science.* 300:801–805.
16. Dobrzyński, M., and F. J. Bruggeman. 2009. Elongation dynamics shape bursty transcription and translation. *Proc. Natl. Acad. Sci. USA.* 106:2583–2588.
17. Ali, M. Z., S. Choubey, …, R. C. Brewster. 2020. Probing mechanisms of transcription elongation through cell-to-cell variability of RNA polymerase. *Biophys. J.* 118:1769–1781.
18. Wang, J., B. Pfeuty, …, M. Lefranc. 2014. Minimal model of transcriptional elongation processes with pauses. *Phys. Rev. E - Stat. Nonlinear Soft Matter Phys.* 90:050701.
19. Klumpp, S., and T. Hwa. 2008. Stochasticity and traffic jams in the transcription of ribosomal rna: intriguing role of termination and antitermination. *Proc. Natl. Acad. Sci. USA.* 105:18159–18164.
20. Dong, J., S. Klumpp, and R. K. P. Zia. 2012. Entrainment and unit velocity: surprises in an accelerated exclusion process. *Phys. Rev. Lett.* 109:130602.

21. van den Berg, A. A., and M. Depken. 06 2017. Crowding-induced transcriptional bursts dictate polymerase and nucleosome density profiles along genes. *Nucleic Acids Res.* 45:7623–7632.

22. Sevier, S. A., D. A. Kessler, and H. Levine. 2016. Mechanical bounds to transcriptional noise. *Proc. Natl. Acad. Sci. USA.* 113:13983–13988.

23. Sevier, S. A., and H. Levine. 2018. Properties of gene expression and chromatin structure with mechanically regulated elongation. *Nucleic Acids Res.* 46:5924–5934.

24. Ancona, M., A. Bentivoglio, …, D. Marenduzzo. 2019. Transcriptional bursts in a nonequilibrium model for gene regulation by supercoiling. *Biophys. J.* 117:369–376.

25. Chong, S., C. Chen, …, X. S. Xie. 2014. Mechanism of transcriptional bursting in bacteria. *Cell.* 158:314–326.

26. Fujita, K., M. Iwaki, and T. Yanagida. 2016. Transcriptional bursting is intrinsically caused by interplay between RNA polymerases on DNA. *Nat. Commun.* 7:13788.

27. Tantale, K., F. Mueller, …, E. Bertrand. July 2016. A single-molecule view of transcription reveals convoys of RNA polymerases and multi-scale bursting. *Nat. Commun.* 7:12248.

28. Ma, J., L. Bai, and M. D. Wang. 2013. Transcription under torsion. *Science.* 340:1580–1583.

29. Chatterjee, P., N. Goldenfeld, and S. Kim. 2021. Dna supercoiling drives a transition between collective modes of gene synthesis. *Phys. Rev. Lett.* 127:218101.

30. Tripathi, S., S. Brahmachari, …, H. Levine. 2022. DNA supercoiling-mediated collective behavior of co-transcribing RNA polymerases. *Nucleic Acids Res.* 50:1269–1279, gkab1252.

31. Dorman, C. J., and M. J. Dorman. June 2016. DNA supercoiling is a fundamental regulatory principle in the control of bacterial gene expression. *Biophys. Rev.* 8:209–220.

32. Marko, J. F., and E. D. Siggia. 1994. Bending and twisting elasticity of dna. *Macromolecules.* 27:981–988.

33. Laleman, M., M. Baiesi, …, E. Carlon. 2016. Torque-induced rotational dynamics in polymers: torsional blobs and thinning. *Macromolecules.* 49:405–414.

34. Brackley, C. A., J. Johnson, …, D. Marenduzzo. 2016. Stochastic model of supercoiling-dependent transcription. *Phys. Rev. Lett.* 117:018101.

35. Le, T. B., and M. T. Laub. 2016. Transcription rate and transcript length drive formation of chromosomal interaction domain boundaries. *EMBO J.* 35:1582–1595.

36. Marko, J. F. 2007. Torque and dynamics of linking number relaxation in stretched supercoiled dna. *Phys. Rev. E - Stat. Nonlinear Soft Matter Phys.* 76:021926.

37. Wolgemuth, C. W., T. R. Powers, and R. E. Goldstein. 2000. Twirling and whirling: viscous dynamics of rotating elastic filaments. *Phys. Rev. Lett.* 84:1623–1626.

38. Powers, T. R. 2010. Dynamics of filaments and membranes in a viscous fluid. *Rev. Mod. Phys.* 82:1607–1631.

39. Wada, H., and R. R. Netz. 2006. Non-equilibrium hydrodynamics of a rotating filament. *Europhys. Lett.* 75:645–651.

40. Revyakin, A., R. H. Ebright, and T. R. Strick. 2004. Promoter unwinding and promoter clearance by rna polymerase: detection by single-molecule dna nanomanipulation. *Proc. Natl. Acad. Sci. USA.* 101:4776–4780.

41. Wang, J. C. 1996. Dna topoisomerases. *Annu. Rev. Biochem.* 65: 635–692.

42. Bush, N. G., K. Evans-Roberts, and A. Maxwell. Oct. 2015. DNA topoisomerases. *EcoSal Plus.* 6.

43. Joshi, R. S., B. Piña, and J. Roca. 06 2012. Topoisomerase II is required for the production of long Pol II gene transcripts in yeast. *Nucleic Acids Res.* 40:7907–7915.

44. Wang, Y., S. Rakela, …, F. Leng. 2019. Kinetic study of DNA topoisomerases by supercoiling-dependent fluorescence quenching. *ACS Omega.* 4:18413–18422.

45. Wu, H.-Y., J. Tan, and M. Fang. 1995. Long-range interaction between two promoters: activation of the leu-500 promoter by a distant upstream promoter. *Cell.* 82:445–451.

46. Yeung, E., A. J. Dy, …, R. M. Murray. 2017. Biophysical constraints arising from compositional context in synthetic gene networks. *Cell Systems.* 5:11–24.e12.

47. Friedman, L. J., and J. Gelles. 2012. Mechanism of transcription initiation at an activator-dependent promoter defined by single-molecule observation. *Cell.* 148:679–689.

48. Johnstone, C. P., and K. E. Galloway. 2022. Supercoiling-mediated feedback rapidly couples and tunes transcription. Preprint at bioRxiv. https://doi.org/10.1101/2022.04.20.488937.

49. Geng, Y., C. H. Bohrer, …, E. Roberts. 2021. A spatially resolved stochastic model reveals the role of supercoiling in transcription regulation. Preprint at bioRxiv. https://doi.org/10.1101/2021.12.29.474406.

50. Kouzine, F., A. Gupta, …, D. Levens. Mar. 2013. Transcription-dependent dynamic supercoiling is a short-range genomic force. *Nat. Struct. Mol. Biol.* 20:396–403.

51. Liu, J., D. Hansen, …, H. G. Garcia. 2021. Real-time single-cell characterization of the eukaryotic transcription cycle reveals correlations between rna initiation, elongation, and cleavage. *PLoS Comput. Biol.* 17:e1008999.

52. Morrison, M., M. Razo-Mejia, and R. Phillips. 2021. Reconciling kinetic and thermodynamic models of bacterial transcription. *PLoS Comput. Biol.* 17:e1008572–e1008630.